



Photoelectrochemical Water Vapor Splitting Using an Ionomer-Coated Rutile TiO₂ Thin Layer on Titanium Microfiber Felt as an Oxygen-Evolving Photoanode

Journal:	<i>Sustainable Energy & Fuels</i>
Manuscript ID	SE-ART-05-2019-000292.R1
Article Type:	Paper
Date Submitted by the Author:	02-Jun-2019
Complete List of Authors:	Amano, Fumiaki; The University of Kitakyushu, Department of Chemical and Environmental Engineering Mukohara, Hyosuke; The University of Kitakyushu, Department of Chemical and Environmental Engineering Sato, Hiroki; The University of Kitakyushu, Department of Chemical and Environmental Engineering ohno, teruhisa; Kyushu Institute of Technology

ARTICLE

Photoelectrochemical Water Vapor Splitting Using an Ionomer-Coated Rutile TiO₂ Thin Layer on Titanium Microfiber Felt as an Oxygen-Evolving Photoanode

Received 00th January 20xx,
Accepted 00th January 20xx

DOI: 10.1039/x0xx00000x

Fumiaki Amano,^{*ab} Hyosuke Mukohara,^a Hiroki Sato,^a and Teruhisa Ohno^c

Photoelectrochemical (PEC) decomposition of water at room temperature and separation of hydrogen and oxygen has been achieved using a solid-state cell with a proton exchange membrane (PEM). The PEM-PEC cell can use water vapor instead of liquid aqueous electrolytes for solar hydrogen production. In this study, we aimed to evaluate the performance of thermally oxidized rutile TiO₂ layers on titanium microfiber felt for the photoanodic oxidation of water vapor in the gas phase. We investigated the effects of perfluorosulfonic acid ionomer coating, the wavelength and intensity of incident UV light, and external electric bias on the photocurrent density of TiO₂ photoanodes in a humidified gaseous condition. The gas-phase PEC performance of the rutile TiO₂ thin layer electrode was much higher than that of the anatase TiO₂ nanotube array electrode under 385-nm UV illumination at high irradiance (40 mW cm⁻²). The H₂ evolution rate in the PEM-PEC cell using a rutile TiO₂ layer as an oxygen-evolving photoanode was 330 μmol h⁻¹ under 385-nm UV (irradiation area 16 cm²) at an applied voltage of 1.2 V.

Introduction

Photoelectrochemical (PEC) water decomposition is a method for large-scale solar energy conversion into hydrogen (H₂) as a storable and transportable fuel.¹⁻⁴ In the PEC system, H₂ and oxygen (O₂) are easily separated by a membrane because the reactions take place on different electrodes, in contrast to the case of powdered photocatalysts.⁵⁻⁸ Research on PEC water splitting has usually been performed in liquid aqueous electrolytes. However, water supply could be a big issue in practical operation in water-scarce areas such as deserts with long sunshine hours. Currently, gaseous water has been attracting attention as an alternative water resource for water-splitting facilities.⁹⁻¹² Water vapor, which is present as humidity in ambient air, could potentially reduce the cost of the liquid water supply in PEC systems.

For the gas-phase operation, the electrolyte should be a solid membrane such as a proton conducting polymer.^{10, 13-18} However, it was previously shown that the performances of all solid PEC cells under purely gaseous conditions were lower than those of conventional aqueous electrolytes.^{10, 13-16} One of the reasons was the slow kinetics of proton conduction on the photoelectrode surface in the absence of an electrolyte. Amano et al. have found that the gas-polymer electrolyte-

semiconductor triple-phase boundary of nanostructured macroporous photoelectrodes is important for the PEC reaction at the gas-solid interface.¹⁹⁻²¹ A surface coating of Nafion perfluorosulfonic acid ionomer as a proton conducting polymer markedly enhanced the photocurrent of a TiO₂ nanotube array (TNTA) electrode in PEC oxidation of water vapor.²¹

The ionomer-coated anatase TNTA photoanode exhibited an incident photon-to-current conversion efficiency (IPCE) of 26% at an applied voltage (ΔE) of 1.2 V under 365-nm ultraviolet (UV) irradiation.²¹ The photoanode induced oxidation of water vapor by photogenerated holes to form O₂ and protons (2H₂O + 4h⁺ → O₂ + 4H⁺). The PEC oxidation of water vapor was even induced under atmospheric pressure air. The protons are transported through a proton exchange membrane (PEM) and reduced to H₂ over a Pt catalyst cathode using photogenerated electrons, which pass through the outer circuit (2H⁺ + 2e⁻ → H₂). The H₂ production rate was 600 μmol h⁻¹ in a PEM-PEC cell (irradiance I₀ = 40 mW cm⁻², irradiation area 16 cm²) using an anatase TNTA photoanode.²¹ However, the bandgap photoexcitation of anatase TiO₂ is achieved only under UV irradiation ($\lambda < 388$ nm, 3.2 eV).

Rutile TiO₂, which is a polymorph of titanium(IV) oxide, is an efficient water oxidation photocatalyst.^{22, 23} It possesses a band gap 3.0 eV narrower than that of anatase. The conduction band edge of rutile is more positive than that of anatase by about 0.2 eV.²⁴ This photoabsorption (wavelength, $\lambda < 413$ nm) is an advantage of rutile TiO₂ compared with anatase TiO₂. However, the photoactivities of rutile TiO₂ are frequently lower than those of anatase TiO₂ in many photocatalytic applications. In contrast, recent publications show that partly reduced rutile TiO₂ exhibits high photocatalytic activity.^{25, 26} Further, rutile TiO₂

^a Department of Chemical and Environmental Engineering, The University of Kitakyushu, Kitakyushu, Fukuoka 808-0135, Japan

^b Precursory Research for Embryonic Science and Technology (PRESTO), Japan Science and Technology Agency (JST), Kawaguchi, Saitama 332-0012, Japan

^c Department of Applied Chemistry, Kyushu Institute of Technology, Kitakyushu, Fukuoka 804-8550, Japan

Electronic Supplementary Information (ESI) available: [details of any supplementary information available should be included here]. See DOI: 10.1039/x0xx00000x

electrodes have been reported to display high PEC performance in water oxidation.²⁷⁻²⁹

In this study, we focused on rutile TiO₂ photoanodes for PEC water vapor splitting into H₂ and O₂ (see Figure S1 in Supporting Information). Titanium microfiber felts with a three-dimensional network structure have been used as a conductive substrate as the photoanode in a PEM-PEC cell should be porous to facilitate gas diffusion and proton transport in the vertical direction.^{17-21, 30, 31} Tsampas et al. reported that the anatase phase of TiO₂ photoanodes prepared on Ti microfiber felt was more active compared with the rutile phase under 365-nm illumination in the gas-phase PEC reaction.^{17, 31} Herein, we represent that rutile TiO₂ thin layer photoanodes show a much higher photocurrent than that of anatase TiO₂ under 385-nm illumination owing to the difference in the band gaps (3.0 and 3.2 eV). The PEC water vapor splitting over the thermally-oxidized rutile thin layers was achieved by coating the surface with Nafion perfluorosulfonic acid ionomer. The PEC properties of the TiO₂ electrodes in the gaseous condition were investigated under different reaction conditions such as wavelength and intensity of incident light and external electric bias to understand the characteristic of the newly developed PEM-PEC cell.

Experimental

Preparation of TiO₂ electrodes

Sintered Ti microfiber felt (thickness 0.1 mm, porosity 67%, Nikko Techno, Japan) was used as the conductive material for the TiO₂ electrodes. After ultrasonic cleaning in acetone and deionized water, the Ti microfiber felt was calcined in the air using an electric muffle furnace at different temperatures (450–750°C) for several hours (1, 2 and 3 h). During the calcination, the TiO₂ layer is formed on the microfiber surface by thermal oxidation of Ti in the presence of O₂. The obtained thermally oxidized TiO₂ layer on the Ti microfiber was coated with a drop of Nafion perfluorosulfonic acid ionomer dispersion (5 wt% in 50 wt% alcohols and 45 wt% water, Sigma–Aldrich Japan, Japan). The drop casting (5 μL cm⁻² for each of the front and back sides) was repeated several times after drying at 80°C. Anatase TNTA was prepared by anodization of the Ti microfiber felt in ethylene glycol containing fluorine and water at 50 V for 3 h and subsequent calcination in the air at 550°C for 2 h.^{21, 27}

Characterization

X-ray diffraction (XRD) measurements were carried out on a SmartLab diffractometer (Rigaku, Japan) using Cu Kα radiation at 45 kV and 200 mA. Laser Raman spectra were recorded on an NRS-5100 spectrometer (JASCO, Japan) using 532-nm green radiation. Scanning electron microscope (SEM) observation and energy dispersive X-ray spectroscopy (EDS) analysis were performed with a JSM-7800F microscope (JEOL, Japan). The SEM images were obtained at a working distance of 10 mm and an acceleration voltage of 10 kV.

PEC measurements in aqueous electrolyte

A conventional three-electrode system was used in a one-compartment glass reactor. The electrolyte was an aqueous solution of 0.2 mol L⁻¹ sodium sulfate (Na₂SO₄) and 0.1 mol L⁻¹ sodium phosphate buffer with a pH of 6.7. The solution was purged with argon (20 mL min⁻¹). The reference electrode was a silver/silver chloride (Ag/AgCl), and the potential versus RHE (E_{RHE}) was obtained by the equation, $E_{\text{RHE}} = E_{\text{Ag/AgCl}} + 0.059 \text{ pH} + 0.195$. Photoirradiation was performed using a UV light-emitting diode (LED, central $\lambda = 365 \text{ nm}$, Nitride Semiconductor, Japan) and a 300-W xenon lamp with bandpass filters (Asahi Spectra, Japan) at room temperature. The irradiation area of the photoanode was adjusted to 1 cm². The intensity of the incident light was measured by an optical power meter (Hioki, Japan). IPCE was calculated from photocurrent density (J_{photo}) [mA cm⁻²] and I_0 [mW cm⁻²] at λ [nm] using the equation, $\text{IPCE} = (1240/\lambda) \times J_{\text{photo}} / I_0$.

A Mott-Schottky plot was recorded on a VersaSTAT 4 potentiostat with a frequency response analyser (Ametek, USA). The space charge layer capacitance (C) was measured in the electrolyte in the dark using the electrochemical impedance method at a frequency of 1000 Hz.

Preparation of membrane electrode assemblies

Carbon black-supported platinum nanoparticles (Pt/CB, TEC10E50E, Pt loading 47 wt%, Tanaka Kikinokoku, Japan) were used as the cathode catalyst for H₂ evolution. A mixture of Pt/CB and Nafion ionomer (weight ratio 1 : 1) in propanol was used as the cathode catalyst ink for preparation of ionomer-mixed Pt/CB films (0.1 mg-Pt cm⁻²). To fabricate a membrane electrode assembly (MEA), the ionomer-mixed Pt/CB films and TiO₂ electrodes were hot pressed onto each side of a Nafion N117 membrane (thickness of 183 μm, DuPont, USA) at 140°C with pressures of 15 kN and 10 kN, respectively.

PEC measurements in the gas phase

A two electrode system was used in an H-type dual-compartment glass reactor and a planar-type dual-compartment stainless-steel reactor (see Figure S2). The sizes of the Nafion membrane and electrodes were 40 × 40 mm² and 14 × 14 mm² for the H-type reactor and 80 × 80 mm² and 50 × 50 mm² for the planar-type reactor. The water vapor (3 vol%, relative humidity > 90%) was prepared by passing argon through a bubbler filled with deionized water at room temperature and introduced to the dual compartments with each flow rate of 20 mL min⁻¹. The relative humidity was measured by a humidity transmitter (EE33, E+E Elektronik, Austria). The direct-current voltage between the two electrodes was controlled by the potentiostat. Photoirradiation was performed for the TiO₂ electrodes using UV LEDs (central $\lambda = 365 \text{ nm}$ and 385 nm). The irradiation area was 2 cm² for the H-type reactor and 16 cm² for the planar-type reactor. The exhaust gases were analyzed by online gas chromatographs equipped with a thermal conductivity detector (GC-8A and GC-2014, Shimadzu, Japan). Molecular Sieve 5A and ShinCarbon ST columns were used for the gas separation with argon and helium, respectively, as the carriers gases.

Results and discussion

Figure 1 shows the XRD pattern of the Ti microfiber calcined in the air at 650°C for 2 h, which is denoted as R650 hereafter. The XRD pattern of the Ti microfiber was consistent with that of hexagonal α -Ti (PDF #00-044-1294). After the calcination at 650°C, the peaks assigned to hexagonal α -Ti broadened and the peaks assigned to rutile TiO_2 (PDF #00-021-1276) emerged. The broadening is due to the formation of hexagonal Ti_3O (PDF #01-073-1583) (see Figure S3). Raman spectrum of R650 displayed bands at 606, 437, and 239 cm^{-1} , which are assigned to the A_{1g} mode, E_g mode, and second-order scattering of rutile TiO_2 , respectively.³² The rutile TiO_2 phase was obtained by thermal oxidation of Ti microfiber felt.

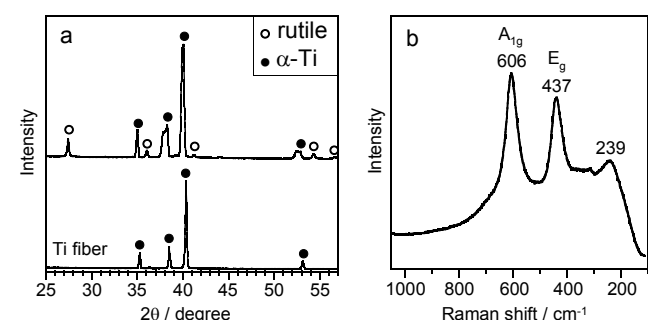


Figure 1. (a) XRD pattern and (b) Raman spectrum of Ti microfiber after calcination in the air at 650°C for 2 h. The XRD pattern of pristine Ti microfiber is translated in the y-axis direction for clarity.

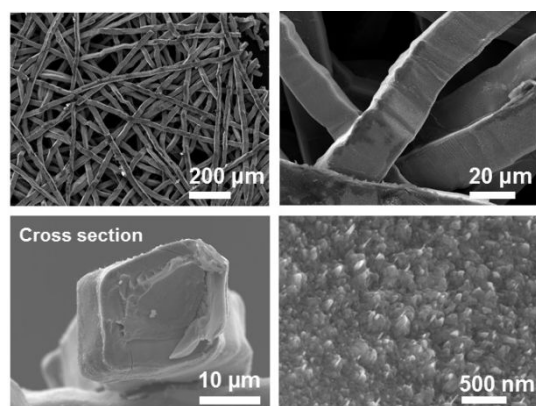


Figure 2. SEM images of the rutile TiO_2 layer on Ti microfiber calcined in air at 650°C for 2 h (R650).

Figure 2 shows SEM images of the rutile TiO_2 layer on R650. The macrostructure of the microfiber felt was not changed by calcination at 650°C. The microfibers are folded to form a network-like structure with macroporous void spaces. The porous structure will be an essential property for their use as a substrate of gas diffusion electrodes. The cross-sectional images show square-like shapes with diameters of about 20 μm . The surface nanostructure changed from a flat to a grainy texture after the formation of rutile TiO_2 . Needle-like nanostructures were observed in some parts of the surface.

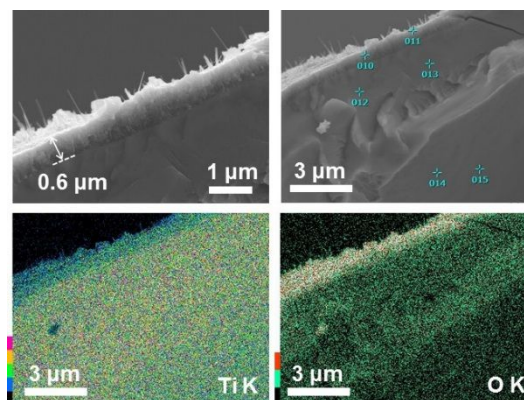


Figure 3. SEM images and EDS elemental (titanium and oxygen) mappings for the cross-section surface of the rutile TiO_2 layer on R650. The element concentration is indicated by the colour bar located at the left bottom of each map.

Figure 3 shows the results of EDS elemental analysis of the cut surface of the thermally oxidized Ti fiber. The cross-sectional SEM image shows that the thickness of the TiO_2 layer was about 0.6 μm . The atomic percentages of Ti and O were 20%–30% and 60%–70% at the surface region and 70%–80% and 10%–15% at the bulk, which was exposed by the cutting. Carbon was detected as an impurity from the carbon tape for sample adhesion. The formation of the thermally oxidized layer on the Ti surface was confirmed by the oxygen-enriched region at the boundary. The Ti-K and O-K elemental mapping images clearly showed the oxygen-enriched thin layer around the square cross-section of the microfibers.

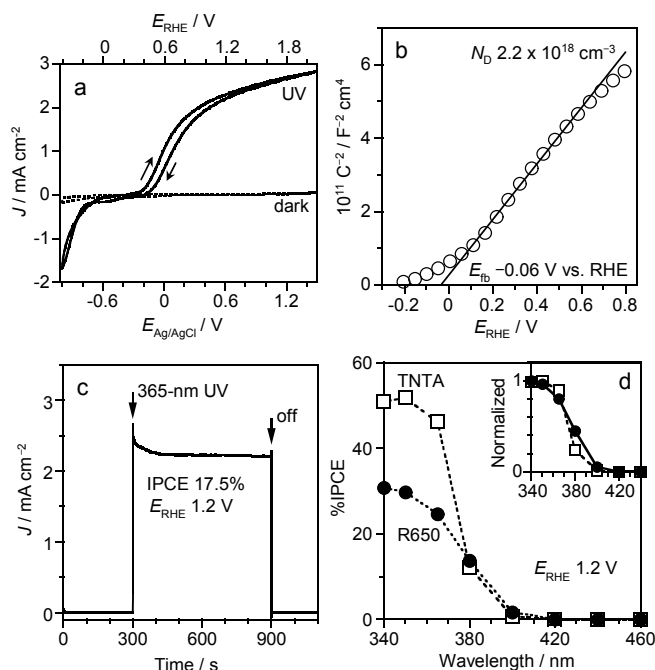


Figure 4. PEC properties of TiO_2 electrodes in a pH 6.7 aqueous electrolyte. (a) Current density (J) vs. potential curves of R650 in the dark and under 365-nm UV ($I_0 = 43 \text{ mW cm}^{-2}$) in cyclic voltammetry. (b) Mott-Schottky plot of R650 in the dark. (c) Photocurrent response of R650 at 1.2 V vs. RHE under the 365-nm UV irradiation. (d) IPCE action spectra of R650 and anatase TNTA electrodes at E_{RHE} of 1.2 V. Inset shows the normalized action spectra.

PEC properties of R650 were investigated by a three-electrode configuration in a conventional aqueous electrolyte (pH 6.7). The cyclic voltammograms of R650 (Figure 4a) show the negligible current in dark and anodic current under UV irradiation. This behavior agreed with the typical behavior of n-type semiconductor electrodes under anodic polarization. The photocurrent onset potential was about -0.3 V vs. Ag/AgCl in the forward scan, indicating that water oxidation was induced at $E_{\text{RHE}} > +0.3$ V under UV irradiation. The photocurrent was increased by calcination at 650°C for 2 h accompanied by the formation of the rutile TiO_2 crystallites (see Figure S3 and S4). The microfiber felt calcined at 750°C for 2 h was difficult to apply to the electrode because it exhibited brittle behaviour.

Figure 4b shows a plot of $1/C^2$ of R650 in the applied potential function. Flatband potential (E_{FB}) was determined by using the Mott-Schottky equation, $1/C^2 = (2/(q \epsilon \epsilon_0 N_D)) (E - E_{\text{fb}} - kT/q)$, where q is the elementary electric charge, ϵ is the dielectric constant, ϵ_0 is the permittivity of the vacuum and kT/q is the thermal voltage. The E_{FB} of R650 was -0.06 V vs. RHE, which was similar to the reported values for rutile TiO_2 .^{23, 24, 33} The difference between the E_{FB} and the photocurrent onset potential ($E_{\text{RHE}} = 0.3$ V) is an overpotential required to suppress the fast recombination of photoexcited electron and hole. The donor density (N_D) of the n-type semiconductor was calculated from the positive slope to be $2.2 \times 10^{18} \text{ cm}^{-3}$ using an ϵ of 86 for the rutile TiO_2 . The N_D value was similar to the reported values of TiO_2 electrodes.³³

Figure 4c shows steady-state J_{photo} of R650 at 1.2 V vs. RHE under 365-nm UV ($I_0 = 43 \text{ mW cm}^{-2}$). The IPCE was calculated to be 17.5%. This efficiency was lower than the IPCE of an anatase TNTA electrode (26.5%) measured under the same conditions.²¹ Figure 4d shows the action spectra of IPCE at λ of the incident light. The IPCE of TNTA was higher than that of R650 at $\lambda \leq 370$ nm, whereas there was no significant difference at 385 nm (12.2% for TNTA and 13.7% for R650). In the normalized action spectra, the onset of IPCE was estimated to be 385 nm and 405 nm, which corresponds to 3.22 eV and 3.06 eV for TNTA and R650, respectively. The energies are similar to the reported band gaps of anatase (3.2 eV) and rutile (3.0 eV), respectively.²³

The R650 photoanode was applied to a PEM-PEC cell for a water vapor splitting reaction. Nafion ionomer-mixed Pt/CB catalyst film was used as an H_2 -evolving cathode. The MEA composed of a photoanode, a Nafion membrane, and a cathode was installed in an H-type dual-compartment glass reactor (Figure S2a, irradiation area 2 cm^2). The PEC properties were investigated using a two electrode configuration under continuous flows of humidified argon into the two compartments at room temperature.

Figure 5a shows the cyclic voltammograms of the MEA in the 3 vol% water vapor flow. There is no chemical potential difference between the two compartments. The current response was negligible in the dark. We confirmed that bare R650 exhibited a photocurrent response under the gas-phase conditions, but the J_{photo} was small compared with that in the aqueous electrolyte. Herein, we found that the drop casting of a Nafion perfluorosulfonic acid ionomer dispersion on R650 drastically enhanced the J_{photo} of the MEA. The enhanced J_{photo}

by Nafion ionomer coating was also reported for other semiconductor electrodes.^{20, 21}

Figure 5b shows the steady-state J_{photo} of R650 in the PEM-PEC cell. The ΔE was set to 1.2 V between the O_2 -evolving photoanode and the ionomer-mixed Pt/CB catalyst cathode. The J_{photo} of R650 gradually increased with an increase in the coating time of the 5wt% Nafion ionomer dispersion. The drop amount was $10 \mu\text{L cm}^{-2}$ for each coat. Figure 5c shows the loading of Nafion ionomer determined using an analytical balance. The weight of ionomer loading increased with the number of coating treatments (about 0.5 mg cm^{-2} per coating). Figure 5d summarizes the relationship between the IPCE, which is converted from the steady-state J_{photo} at 1.2 V, and the ionomer loading on the R650. The IPCE was proportional to the ionomer loading below 2.0 mg cm^{-2} and became saturated at the fourth coating. Importantly, the saturated IPCE of 17% was consistent with that of bare R650 in the aqueous electrolyte (Figure 4c). This suggests that the Nafion ionomer coating improved the proton-coupled electron transfer, which was the rate determining step in the gas-phase reaction. It is proposed that solid electrolyte thin film coatings provide a gas-electrolyte-semiconductor triple-phase boundary on the photoanodes.^{20, 21} Nafion ionomer is also adsorbent for a low concentration of water vapor in the gas phase. The hydrated ionomer shows proton conductivity even at room temperature.³⁴

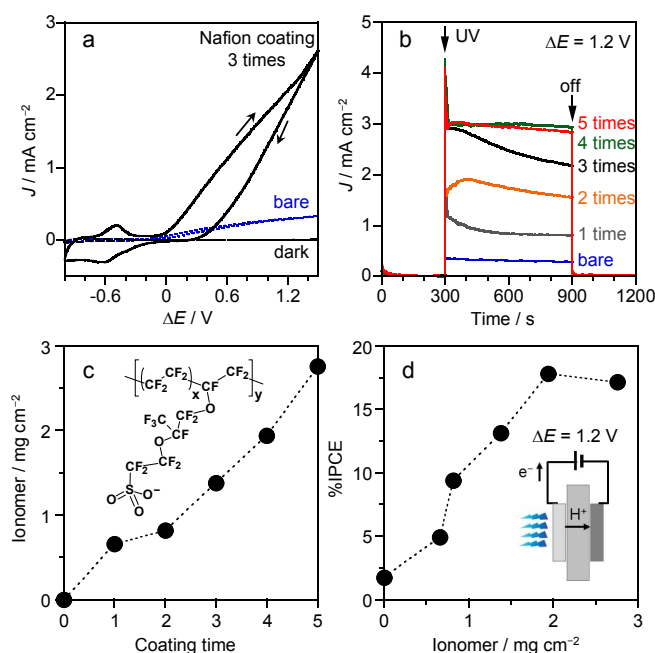


Figure 5. PEC properties of R650 | PEM | Pt/CB in a H-type glass reactor with 3 vol% water vapor. (a) Cyclic voltammograms of bare R650 and Nafion ionomer-coated R650 under 365-nm UV ($I_0 = 43 \text{ mW cm}^{-2}$). (b) Effect of Nafion ionomer coating on the photocurrent at an applied voltage (ΔE) of 1.2 V. (c) Loading amount of Nafion ionomer as a function of the number of coatings. (d) Effect of Nafion ionomer loading on IPCE at a ΔE of 1.2 V.

Figure 6 shows EDS fluorine mapping images of Nafion ionomer-coated R650 microfiber felt. The content of fluorine

and carbon increased with the increase in number of coatings of Nafion ionomer (The molecular structure is shown in the inset of Figure 5c). The mapping image shows that the Nafion ionomer covered the microfibers and some of the polymer electrolytes aggregated in the void spaces at the intersection of the microfibers. The coating was not homogeneous, but the microfibers were almost covered by the ionomer after three coating treatments. The electrolyte covers not only the surface but also the middle part of the microfiber felt (Figure S5).

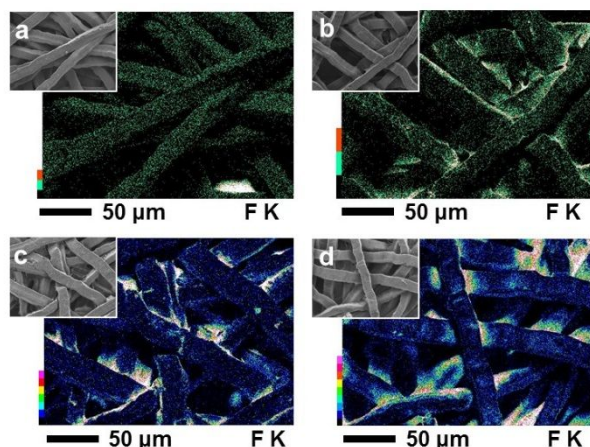


Figure 6. SEM images and EDS elemental (fluorine) mapping images of (a) R650 without Nafion ionomer coating and R650 coated with Nafion ionomer (b) once, (c) twice, and (d) three times.

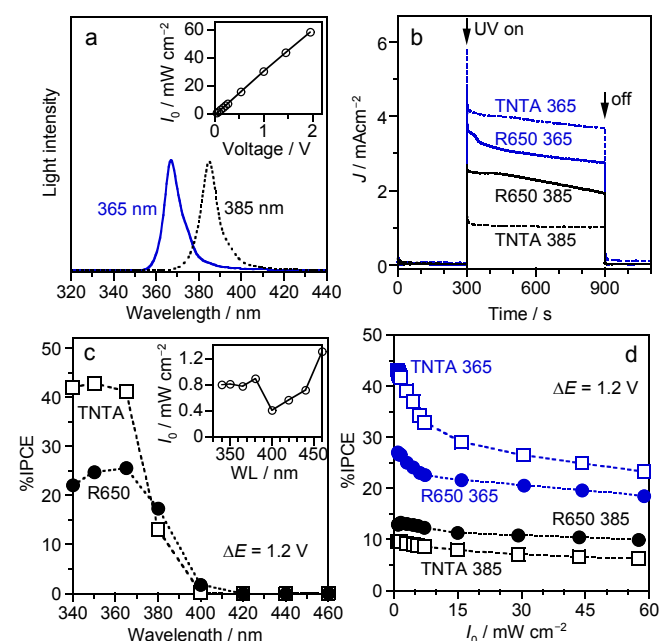


Figure 7. Effect of irradiation wavelength on the photocurrent of ionomer-coated TiO_2 | PEM | Pt/CB in a H-type glass reactor with 3 vol% water vapor. (a) Spectra of 365-nm and 385-nm LEDs. The inset shows the irradiance (I_0) at 365 nm vs. LED forward voltage, (b) Photocurrent response of R650 and TNTA at 1.2 V under 365-nm and 385-nm UV ($I_0 = 40 \text{ mW cm}^{-2}$). (c) IPCE action spectra at 1.2 V. The inset shows the I_0 of monochromatic light for IPCE measurements. (d) Effect of light intensities ($\lambda = 365 \text{ nm}$ and 385 nm) on the IPCE of R650 and TNTA at 1.2 V.

We further investigated the PEC properties of the ionomer-coated R650 in the H-type glass reactor under UV irradiation with different λ and I_0 . Figure 7a shows the spectrum of LEDs with a central λ of 365 nm and 385 nm. The full width at half maximum was about 10 nm. The I_0 was linearly controlled by the LED forward voltage. Figure 7b shows the steady-state J_{photo} of Nafion ionomer-coated TNTA and R650 electrodes under 365-nm and 385-nm UV ($I_0 = 40 \text{ mW cm}^{-2}$). The J_{photo} of TNTA (IPCE = 21%) was higher than that of R650 under 365 nm (IPCE = 16%). However, the trend was reversed under violet light ($\lambda > 380 \text{ nm}$). The IPCE of R650 (11%) was much higher than that of TNTA (5.6%). This is probably because the bandgap of rutile TiO_2 is narrower than that of anatase.

Figure 7c shows IPCE action spectra for the oxidation of water vapor in the PEM-PEC reactor. The spectra in the gas-phase were similar to that in the aqueous electrolyte. The IPCE of R650 (17.4%) was higher than that of TNTA (13.1%) at 385 nm and lower than that at $\lambda \leq 370 \text{ nm}$. The ionomer-coated R650 exhibited a photoresponse even under 400-nm irradiation (IPCE = 1.9%) owing to the bandgap of rutile (3.0 eV). The IPCE of TNTA at 365 nm in the action spectra (41%) was much higher than that recorded under a I_0 of 40 mW cm^{-2} . This was because the IPCE in the action spectra was obtained at a low I_0 (0.8 mW cm^{-2}) as shown in the inset of Figure 7c. The IPCE was found to be decreased with an increase of I_0 (Figure 7d). The decrease of IPCE was significant under 365-nm irradiation compared with 385-nm irradiation. This may be related to the difference in the penetration depth of the light into the semiconductor surface at wavelengths near the band gap. The light penetration depth at 365 nm is shorter than that at 385 nm for anatase TiO_2 (band gap 3.2 eV).^{35,36} Many holes are generated inside the electric field of anatase TNTA (film thickness 5 μm) under 365-nm irradiation with low intensity. The PEC performance of the rutile TiO_2 electrode was comparable with the anatase TNTA electrode at high I_0 (40 mW cm^{-2} , $\lambda = 365 \text{ nm}$).

A planar-type dual-compartment stainless-steel reactor, which has a UV irradiation area of 16 cm^2 (Figure S2b), was used for PEC water vapor splitting to evolve H_2 and O_2 separately. The TNTA and R650 electrodes with four coats of Nafion ionomer were applied to the MEA as O_2 -evolving photoanodes. Figure 8a and Table 1 show that the photocurrent of R650 (IPCE = 8.7%) was higher than that of TNTA (IPCE = 4.8%) at an ΔE of 1.2 V under 385-nm irradiation. The IPCE was lower than that observed in the H-type glass reactor because of the insufficient current collection owing to the increase of the electrode area from 1 cm^2 to 25 cm^2 .

The gases evolved in the photoanode and cathode compartments, which were separated by a Nafion membrane, were analysed by different gas chromatographs. In the cathode compartment, we observed the formation of H_2 as a product (Figure 8b). The H_2 evolution rate was consistent with half of the electron flow ($e^-/2$), which passed through the outer circuit. The current efficiency of H_2 was close to 100% (Faraday efficiency (FE) shown in Table 1). This indicates that the two-electron reduction of protons by photoexcited electrons is promoted on the Pt/C catalyst electrode. The H_2 evolution rate of R650 was $5.5 \mu\text{mol min}^{-1}$, which was about 1.8 times higher than the rate

of the TNTA photoanode, at 1.2 V under 385-nm illumination. The yield of H₂ was calculated to be about 20%, which is the ratio of the H₂ produced from the cathode compartment to the H₂O fed into the photoanode compartment.

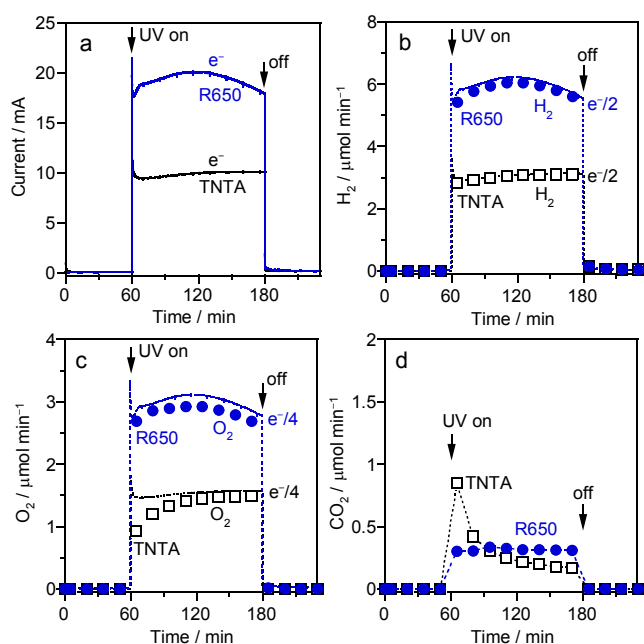


Figure 8. PEC splitting of 3 vol% water vapor by ionomer-coated TiO₂ | PEM | Pt/CB at 1.2 V under 385-nm UV ($I_0 = 40 \text{ mW cm}^{-2}$, area 16 cm^2). (a) Photocurrent response, (b) H₂ formation rate in the cathode compartment, the formation rate of (c) O₂ and (d) CO₂ in the photoanode compartment for R650 and TNTA. The flow rate of the electron (e^-) is divided by the number of electrons required to form a product (2 for H₂ and 4 for O₂).

Table 1. IPCE and Faraday efficiency (FE) for PEC water vapor splitting.^[a]

Photoanode	IPCE (%)	FE of H ₂ (%)	FE of O ₂ (%)
R650	8.7	98	94
TNTA	4.8	99	95

^[a] Ionomer-coated TiO₂ | PEM | Pt/CB at 1.2 V under 385-nm UV ($I_0 = 40 \text{ mW cm}^{-2}$).

In the photoanode compartment (Figure 8c), we observed O₂ evolution by four-electron oxidation of water vapor by photogenerated holes. This indicates that water vapor splitting into H₂ and O₂ was induced in the PEM-PEC cell. However, the O₂ evolution rate was slightly less than one-quarter of the electron flow. The current efficiency of O₂ was 94% for R650. It is suggested that there are side reactions in the photoanode compartment.

We detected carbon dioxide (CO₂) as a byproduct in the photoanode compartment (Figure 8d). The evolved CO₂ is considered to be generated by the decomposition of the Nafion ionomer. The formation rate of CO₂ over R650 was constant in the PEC reaction. This suggests that part of the Nafion ionomer is gradually degraded during the PEC operation in the presence of water vapor. The undesired oxidation of the Nafion ionomer would be promoted by oxidants such as hydroxyl radicals, which can be generated by photogenerated holes ($\text{H}_2\text{O} + h^+ \rightarrow \bullet\text{OH} + \text{H}^+$). In the case of a polymer electrolyte fuel cell, hydroxyl

radicals originating from H₂O₂ are attributed to the oxidant to degrade ionomers.³⁴ The formation rate of CO₂ over TNTA was high immediately after the light was switched on, suggesting the initial formation of $\bullet\text{OH}$ for anatase TiO₂ photoanode.

As CO₂ was detected as a byproduct, we investigated the long-term stability of the PEM-PEC system (see Figure S6). It was demonstrated that the photocurrent and H₂ evolution rate were increased in the beginning and gradually decreased with the PEC operation time. The photocurrent was decreased to one-third of the initial value after PEC water vapor splitting for 20 h (Table S1). The removal of the Nafion ionomer from the electrode surface was confirmed by EDS fluorine mapping (Figure S7). The carbon and fluorine content decreased by half after the PEC reaction (Table S2). The degradation of the Nafion ionomer was also observed in the anatase TNTA photoanode. To improve the stability of the PEM-PEC system for gas phase reactions, it is necessary to suppress the CO₂ formation by improving the reaction selectivity. The photogenerated holes should be used for O₂ evolution reaction without the formation of the oxidants that decompose the ionomer.

Figure 9 shows the effect of external electric bias on the PEC water vapor splitting over the rutile TiO₂ photoanode. The photocurrent was increased with an increase in ΔE . The IPCE was decreased to 1.4 % when ΔE was reduced to 0.6 V (Table 2). The current efficiency of H₂ was 100%, but that of O₂ was 89% suggesting the presence of side reactions at low ΔE . Although the CO₂ evolution rate slightly increased with ΔE , the current efficiency of O₂ was close to 100% at ΔE higher than 0.9 V. These results demonstrate that a relatively high external voltage should be applied to induce overall water splitting into H₂ and O₂ (2 : 1) when using TiO₂ photoanodes. The solar-to-hydrogen efficiency (STH) is calculated from the energy gain of water splitting (reaction Gibbs energy 237 kJ mol^{-1} and theoretical voltage 1.23 V).^{2, 4} When a bias voltage is applied to the PEC systems, the external energy should be subtracted from the energy gain. Therefore, ΔE has to be reduced to improve STH. The development of n-type semiconductor electrodes with negative E_{fb} and low overpotential is a further challenge in developing a PEM-PEC system for water vapor splitting. However, the all solid system has the capability to reduce the energy required to supply liquid water and separate H₂ from O₂.

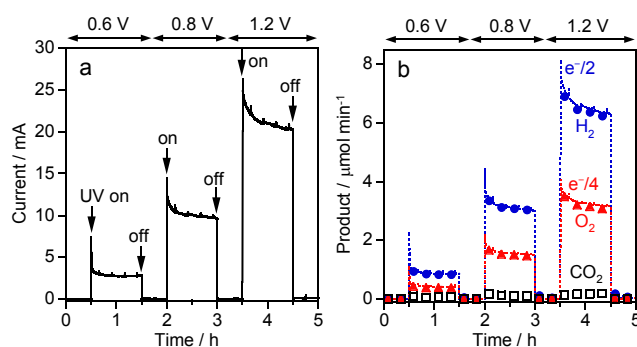


Figure 9. Effect of applied voltage (ΔE) on PEC splitting of 3 vol% water vapor by ionomer-coated R650 | PEM | Pt/CB under 365-nm UV ($I_0 = 40 \text{ mW cm}^{-2}$, area 16

cm²). (a) Photocurrent response. (b) The formation rate of H₂ in the cathode compartment and O₂ and CO₂ in the photoanode compartment.

Table 2. Effect of ΔE on the performances in PEC water vapor splitting.^[a]

$\Delta E / V$	IPCE (%)	FE of H ₂ (%)	FE of O ₂ (%)	CO ₂ / $\mu\text{mol min}^{-1}$
0.6	1.4	100	89	0.07
0.9	5.1	100	97	0.10
1.2	10.7	99	97	0.16

^[a] Ionomer-coated R650 | PEM | Pt/CB under 365-nm UV ($I_0 = 40 \text{ mW cm}^{-2}$, area 16 cm²). FE is Faraday efficiency.

Conclusions

We evaluated the PEC performance of a rutile TiO₂ thin layer, which was handily prepared by thermal oxidation of Ti microfiber felt, for the decomposition of water vapor into O₂ and proton. The macroporous rutile TiO₂ electrode exhibited relatively high PEC properties in an aqueous electrolyte. As reported for anatase TNTA electrode, the photocurrent response in the gas-phase condition was drastically enhanced by the coating of the macroporous surface with Nafion perfluorosulfonic acid ionomer to facilitate proton transport. In the PEM-PEC system (irradiation area 2 cm²), anatase TNTA and rutile TiO₂ electrodes exhibited IPCE of 21% and 16% under 365-nm UV irradiation, whereas the IPCE of the rutile (11%) was much higher than that of the anatase (5.6%) under 385-nm UV irradiation. The action spectra indicate that the enhanced photocurrent response of rutile TiO₂ is consistent with the bandgap energy. The light intensity dependence revealed that the IPCE of anatase TNTA was only high under low I_0 . Overall water vapor splitting into H₂ (FE = 100%) and O₂ (FE = 98%) was successful using the rutile TiO₂ photoanode and Pt/C cathode with the benefit of the perfluorosulfonic acid ionomer coating. However, two problems appeared in the PEM-PEC system in this study. One is the undesired oxidation of the Nafion ionomer into CO₂ during the PEC water-splitting reaction, which resulted in the gradual decrease of the photocurrent. The other is the high voltage required to improve the IPCE and current efficiency. A challenge for the future is developing semiconductor electrodes with higher selectivity and efficiency to establish robust PEC H₂ evolution from water vapor at low applied voltage.

Conflicts of interest

There are no conflicts of interest to declare.

Acknowledgements

This work was supported by the Japan Science and Technology Agency (JST), Precursory Research for Embryonic Science and Technology (PRESTO), grant number JPMJPR15S1 and JPMJPR18T1.

References

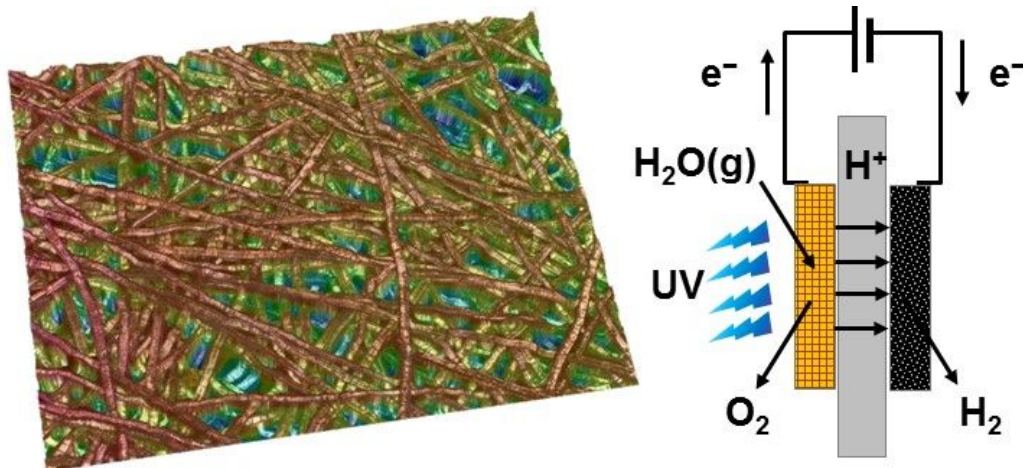
1. A. Fujishima and K. Honda, *Nature*, 1972, **238**, 37-38.
2. M. G. Walter, E. L. Warren, J. R. McKone, S. W. Boettcher, Q. Mi, E. A. Santori and N. S. Lewis, *Chem. Rev.*, 2010, **110**, 6446-6473.
3. K. Maeda, *J. Photochem. Photobiol., C*, 2011, **12**, 237-268.
4. T. Hisatomi, J. Kubota and K. Domen, *Chem. Soc. Rev.*, 2014, **43**, 7520-7535.
5. J. R. McKone, N. S. Lewis and H. B. Gray, *Chem. Mater.*, 2013, **26**, 407-414.
6. B. A. Pinaud, J. D. Benck, L. C. Seitz, A. J. Forman, Z. Chen, T. G. Deutsch, B. D. James, K. N. Baum, G. N. Baum, S. Ardo, H. Wang, E. Miller and T. F. Jaramillo, *Energy Environ. Sci.*, 2013, **6**.
7. A. Berger, R. A. Segalman and J. Newman, *Energy Environ. Sci.*, 2014, **7**, 1468-1476.
8. C. Xiang, A. Z. Weber, S. Ardo, A. Berger, Y. Chen, R. Coridan, K. T. Fountaine, S. Haussener, S. Hu, R. Liu, N. S. Lewis, M. A. Modestino, M. M. Shaner, M. R. Singh, J. C. Stevens, K. Sun and K. Walczak, *Angew. Chem. Int. Ed. Engl.*, 2016, **55**, 12974-12988.
9. J. M. Spurgeon and N. S. Lewis, *Energy Environ. Sci.*, 2011, **4**.
10. J. Rongé, S. Deng, S. Pulinthanathu Sree, T. Bosserez, S. W. Verbruggen, N. Kumar Singh, J. Dendooven, M. B. J. Roeffaers, F. Taulelle, M. De Volder, C. Detavernier and J. A. Martens, *RSC Adv.*, 2014, **4**, 29286-29290.
11. M. A. Modestino, M. Dumortier, S. M. Hosseini Hashemi, S. Haussener, C. Moser and D. Psaltis, *Lab Chip*, 2015, **15**, 2287-2296.
12. S. Kumari, R. Turner White, B. Kumar and J. M. Spurgeon, *Energy Environ. Sci.*, 2016, **9**, 1725-1733.
13. J. Georgieva, S. Armyanov, I. Poullos and S. Sotiropoulos, *Electrochem. Commun.*, 2009, **11**, 1643-1646.
14. J. Georgieva, S. Armyanov, I. Poullos, A. D. Jannakoudakis and S. Sotiropoulos, *Electrochem. Solid-State Lett.*, 2010, **13**, P11-P13.
15. K. O. Iwu, A. Galeckas, A. Y. Kuznetsov and T. Norby, *Electrochim. Acta*, 2013, **97**, 320-325.
16. S. W. Verbruggen, M. Van Hal, T. Bosserez, J. Ronge, B. Hauchecorne, J. A. Martens and S. Lenaerts, *ChemSusChem*, 2017, **10**, 1413-1418.
17. T. Stoll, G. Zafeiropoulos and M. N. Tsampas, *Int. J. Hydrogen Energy*, 2016, **41**, 17807-17817.
18. T. Stoll, G. Zafeiropoulos, I. Dogan, H. Genuit, R. Lavrijsen, B. Koopmans and M. N. Tsampas, *Electrochem. Commun.*, 2017, **82**, 47-51.
19. F. Amano, A. Shintani, K. Tsurui, H. Mukohara, T. Ohno and S. Takenaka, *ACS Energy Letters*, 2019, **4**, 502-507.
20. F. Amano, A. Shintani, H. Mukohara, Y. M. Hwang and K. Tsurui, *Front Chem*, 2018, **6**, 598.
21. F. Amano, H. Mukohara, A. Shintani and K. Tsurui, *ChemSusChem*, 2018, DOI: 10.1002/cssc.201802178.
22. A. Miyoshi, S. Nishioka and K. Maeda, *Chem. Eur. J.*, 2018, **24**, 18204-18219.
23. A. Fujishima, X. Zhang and D. A. Tryk, *Surf. Sci. Rep.*, 2008, **63**, 515-582.
24. L. Kavan, M. Grätzel, S. E. Gilbert, C. Klemenz and H. J. Scheel, *J. Am. Chem. Soc.*, 1996, **118**, 6716-6723.
25. F. Amano, M. Nakata, A. Yamamoto and T. Tanaka, *J. Phys. Chem. C*, 2016, **120**, 6467-6474.
26. F. Amano, M. Nakata, A. Yamamoto and T. Tanaka, *Catal. Sci. Tech.*, 2016, **6**, 5693-5699.
27. F. Amano, H. Mukohara and A. Shintani, *J. Electrochem. Soc.*, 2018, **165**, H3164-H3169.
28. G. Wang, H. Wang, Y. Ling, Y. Tang, X. Yang, R. C. Fitzmorris, C. Wang, J. Z. Zhang and Y. Li, *Nano Lett.*, 2011, **11**, 3026-3033.

ARTICLE

Journal Name

29. C. Yang, Z. Wang, T. Lin, H. Yin, X. Lü, D. Wan, T. Xu, C. Zheng, J. Lin, F. Huang, X. Xie and M. Jiang, *J. Am. Chem. Soc.*, 2013, **135**, 17831-17838.
30. F. Amano, A. Shintani, K. Tsurui and Y.-M. Hwang, *Mater. Lett.*, 2017, **199**, 68-71.
31. G. Zafeiropoulos, T. Stoll, I. Dogan, M. Mamlouk, M. C. M. van de Sanden and M. N. Tsampas, *Sol. Energy Mater. Sol. Cells*, 2018, **180**, 184-195.
32. U. Balachandran and N. G. Eror, *J. Solid State Chem.*, 1982, **42**, 276-282.
33. H. P. Maruska and A. K. Ghosh, *Sol. Energy*, 1978, **20**, 443-458.
34. A. Kusoglu and A. Z. Weber, *Chem. Rev.*, 2017, **117**, 987-1104.
35. I. Cesar, K. Sivula, A. Kay, R. Zboril and M. Grätzel, *J. Phys. Chem. C*, 2009, **113**, 772-782.
36. A. Paracchino, J. C. Brauer, J.-E. Moser, E. Thimsen and M. Graetzel, *J. Phys. Chem. C*, 2012, **116**, 7341-7350.

A table of contents entry: graphic maximum size 8 cm x 4 cm and one sentence of text (maximum 20 words).



Rutile TiO₂ thin layers on titanium microfiber electrode split water vapor into hydrogen and oxygen via a proton exchange membrane.